Anomalous Thermal Expansion in Ising-like Puckered Sheets

Paul Z. Hanakata,* Abigail Plummer, and David R. Nelson
Department of Physics, Harvard University, Cambridge, Massachusetts 02138, USA

(Received 8 June 2021; accepted 27 January 2022; published 17 February 2022)

Motivated by efforts to create thin nanoscale metamaterials and understand atomically thin binary monolayers, we study the finite temperature statistical mechanics of arrays of bistable buckled dilations embedded in free-standing two-dimensional crystalline membranes that are allowed to fluctuate in three dimensions. The buckled nodes behave like discrete, but highly compressible, Ising spins, leading to a phase transition at T_c with singularities in the staggered "magnetization," susceptibility, and specific heat, studied via molecular dynamics simulations. Unlike conventional Ising models, we observe a striking divergence and sign change of the coefficient of thermal expansion near T_c caused by the coupling of flexural phonons to the buckled spin texture. We argue that a phenomenological model coupling Ising degrees of freedom to the flexural phonons in a thin elastic sheet can explain this unusual response.

DOI: 10.1103/PhysRevLett.128.075902

In recent decades, metamaterials with unique properties, such as auxetic behavior and extreme stretchability, have been realized at the macroscale [1,2] as well as the nanoscale [3–7]. More recently, there has been growing interest in designing mechanical materials with programmable memory, using multistable buckled materials [1,8–12] and origami [13–16].

Buckled configurations have also been found (via either first-principles simulations or experiments) in atomically thin materials such as stanene, SnO, PbS, and borophane polymorphs [17–23], as well as in graphene with topological defects or substitutional impurities [24–27]. At the nanoscale, thermal fluctuations can strongly influence any mechanical memories stored in the material as the energy barriers between bistable states become comparable to the temperature. Furthermore, thermal fluctuations also profoundly change the mechanics of atomically thin materials at long wavelengths [3,28–33]. Yet, few studies exist on the interplay between microstructure (e.g., defects) and thermal fluctuations in these atomically thin materials.

We study here the thermal response and phase transitions of puckered sheets with square arrays of buckled positive and negative dilational defects using molecular dynamics simulations. We find that puckered membranes undergo highly compressible Ising-like phase transitions. We also observe an anomalous thermal expansion, where the typically negative coefficient of thermal expansion briefly becomes positive close to the transition, which we explain with a theoretical model coupling spin and elastic degrees of freedom. Creating a highly tunable coefficient of thermal expansion, spanning both positive and negative values, is a goal of many metamaterial design efforts, and we are not aware of any other physically realizable 2D material expected to have this property [34–36]. This unusual anomaly could, for example, be leveraged to create nanoscale device components whose dimensions are insensitive to thermal changes at a particular operating temperature.

The model.—Since *ab initio* molecular dynamics [37] are computationally expensive for studying phase transitions and atomistic potentials for puckered materials are not yet developed, we use a coarse-grained discrete membrane model [38], tuned to approximate an isotropic elastic sheet in the continuum limit. Nodes are connected by harmonic springs [Fig. 1(a)] and there is an energetic cost when the normals of neighboring planes are not aligned [Fig. 1(b)]. The total energy, adapted from Ref. [38], is given by

$$E = \frac{k}{2}\sum_{\langle i,j\rangle}(|\boldsymbol{r}_i - \boldsymbol{r}_j| - a_{ij})^2 + \hat{\kappa}\sum_{\langle \alpha,\beta\rangle}(1 - \boldsymbol{n}_\alpha \cdot \boldsymbol{n}_\beta), \quad (1)$$

where k is the spring constant, $\hat{\kappa}$ is the microscopic bending rigidity, and a_{ij} is the rest length between two connected nodes, i and j. The first sum is over connected nodes and the second sum is over neighboring triangular planes. This model (with $a_{ij} = a_0$, nodes on a triangular lattice) has been shown to produce mechanical [25] and thermal properties [29,30] as well as height-height correlation functions [39] consistent with simulation results of 2D materials (e.g., graphene and MoS_2) using atomistic potentials [25,40,41] (Supplemental Material, Sec. VII) [42]. Furthermore, anticipating our observations of critical phenomena, we expect aspects of the behavior of the system to be insensitive to microscopic details due to universality.

In this Letter, the nodes are arranged on a square lattice and the dilation sites $\mathcal{B}$ are embedded into a background matrix of standard, undilated sites $\mathcal{A}$. The dilations are modeled by changing the preferred lengths of the bonds between $\mathcal{A}$ and $\mathcal{B}$ sites [11], mimicking buckled

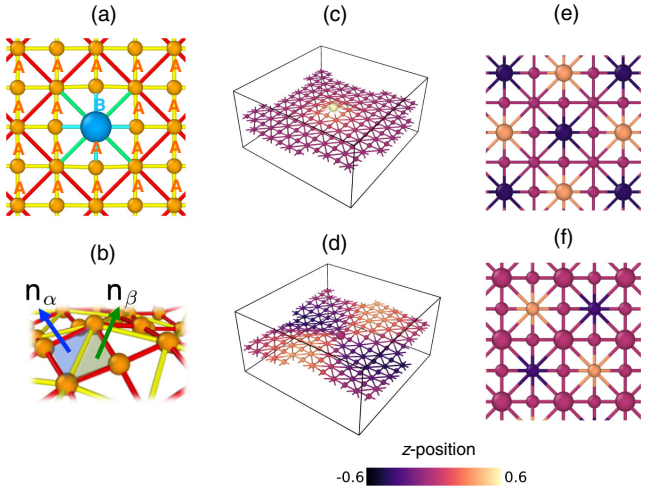

FIG. 1. (a) Square lattice model with background sites $\mathcal{A}$ and a single dilation site $\mathcal{B}$. (b) Schematic of normals of two neighboring triangular plaquettes α and β. (c),(d) Height profiles of relaxed membranes with a single (c) positive and (d) negative dilation at $T = 0$. The color represents the height relative to the zero plane in units of the lattice spacing a_0. The dilation nodes are indicated with a larger radius sphere. (e),(f) Top views of membranes with a square array of positive (e) and negative (f) dilations in a (0, 2) array at $T = 0$. Both display a checkerboard configuration characteristic of antiferromagnetism at $T = 0$ when spins are defined as the nodes that buckle out of plane. Node positions are visualized using OVITO software [50].

monolayers (e.g., SnO and PbS [18,21]). The rest lengths are $a_{\mathcal{AA}} = a_0$, $\bar{a}_{\mathcal{AA}} = a_0\sqrt{2}$, $a_{\mathcal{AB}} = a_0(1+\epsilon)$, and $\bar{a}_{\mathcal{AB}} = a_0\sqrt{2(1+\epsilon+\epsilon^2/2)}$, where ϵ is the fractional change in the bond length, and $\bar{a}$ denotes a diagonal bond. For pristine membranes, the corresponding continuum Young's modulus is $Y = 4k/3$ and the continuum bending rigidity is $\kappa = \hat{\kappa}$ [11]. The continuum size of the dilation is defined as $\Omega_0 = 4a_0^2\epsilon$ [11]. We choose microscopic elastic parameters $a_0 = 1$, $k = 100$, $\hat{\kappa} = 1$, and $\epsilon = \pm 0.1$. Here we study membranes with dilations that provide positive and negative extra area ($\Omega_0 > 0$ and $\Omega_0 < 0$, respectively) with periodic boundary conditions in the x and y directions. See the Supplemental Material Sec. IV [42] for details on other parameter choices. Related tethered membrane models have been studied before [51–54], but with quenched random disorder rather than regular defect arrays.

Mapping buckled structures to Ising spins.—We first describe the behavior of the model at $T = 0$. As the cost of stretching and/or size of the dilation increases, the system crosses a buckling threshold, and a subset of the nodes will prefer to buckle out of the plane. As shown in Figs. 1(c) and 1(d), the relaxed configurations of isolated buckled positive and negative dilations differ. The positive dilations create localized, peaked structures, and the negative dilations lead to saddlelike deformations. This difference can be understood by considering the angular deficit or surplus at the dilation vertex in the inextensible limit—positive dilations have a local angular deficit (discrete positive Gaussian curvature) and negative dilations have a local angular surplus (discrete negative Gaussian curvature).

Despite these differences, we can assign Ising spin variables to dense, square arrays of either positive or negative dilations. In arrays of positive dilations at $T = 0$, the dilations themselves buckle out of the plane [Fig. 1(e)]. In arrays of negative dilations, the dilations remain in a single plane at $T = 0$, and sites on the lattice dual to the dilation superlattice buckle [Fig. 1(f)]. We assign a spin variable of ± 1 to each buckled site depending on whether the dilation or dual site buckles up or down. At finite temperature, we assign spins using nodes' positions relative to the local planes formed by their neighbors to account for thermal fluctuations. With this mapping, the buckled structures shown in Figs. 1(e) and 1(f) are equivalent to checkerboard spin configurations, mechanical analogs of a nearest-neighbor Ising antiferromagnet (AFM). Our simulations support the conclusion that the AFM state is the lowest energy state for the buckled positive and negative dilation arrays that we study. See the Supplemental Material, Secs. III and V [42] and Ref. [11] for further discussion of the buckling threshold and the ground states of arrays.

Finite temperature simulations.—As we are interested in the interplay between microstructure and temperature, we perform molecular dynamics (MD) simulations of both pristine membranes and membranes with positive and negative dilation defects at finite temperature using HOOMD [55]. The membranes have $L_N \times L_N$ nodes with L_N ranging from 24 to 192. Systems with L_N^2 nodes have $N_I = (L_N^2/4)$ dilations. Temperatures are reported in units of the bending energy ($\hat{\kappa} = 1$). See the Supplemental Material Secs. IV and V [42] for more simulation details.

Magnetic ordering and phase transitions.—The mapping between buckled structures and Ising spins suggests we can observe a "magnetic" phase transition at finite temperature in our MD simulations. We use the staggered magnetization per spin as the order parameter $m_{\mathrm{st}} = (1/N_I)\sum_i s_i(-1)^{x_i+y_i}$, where $s_i = \pm 1$ is the spin on site i, and x_i, y_i are the site indices on a 2D square lattice [Figs. 3(d) and 3(e)]. Figure 2 shows $\langle m_{\mathrm{st}}{}^2\rangle$ for puckered membranes as a function of T. We see clearly that pronounced AFM order for $T < 0.2$ rapidly becomes much smaller for $T > 0.2$. Snapshots of spin configurations for several temperatures are shown in Fig. 2 and the Supplemental Material, Sec. V [42]. Note that in our model the bond topology remains unchanged across the temperature range studied.

In studies of critical phenomena, it is typical to measure diverging quantities such as the magnetic susceptibility χ and specific heat C. Following standard methods [57–59], we calculate the staggered susceptibility as $\chi' = (N_{\mathrm{I}}/k_{\mathrm{B}}T)(\langle m_{\mathrm{st}}{}^2\rangle - \langle|m_{\mathrm{st}}|\rangle^2)$. This computationally convenient quantity differs from the true susceptibility

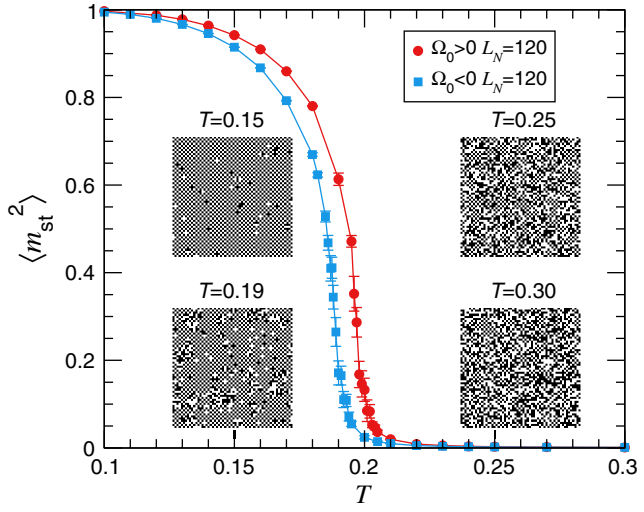

FIG. 2. Squared staggered magnetization $\langle m_{st}^2 \rangle$ as a function of temperature T for $L_N = 120$. Plots for other system sizes can be found in the Supplemental Material, Sec. VI [42]. Error bars are calculated with between 10 and 50 runs, as described in the Supplemental Material, Sec. IV [42]. Jackknife method (see, e.g., Ref. [56]) is used to estimate statistical errors. The insets show snapshots of spin configurations of membranes with positive dilations ($\Omega_0 > 0$) for $T = 0.15$, 0.19, 0.25, and 0.30. The spin configurations for membranes with negative dilations are similar.

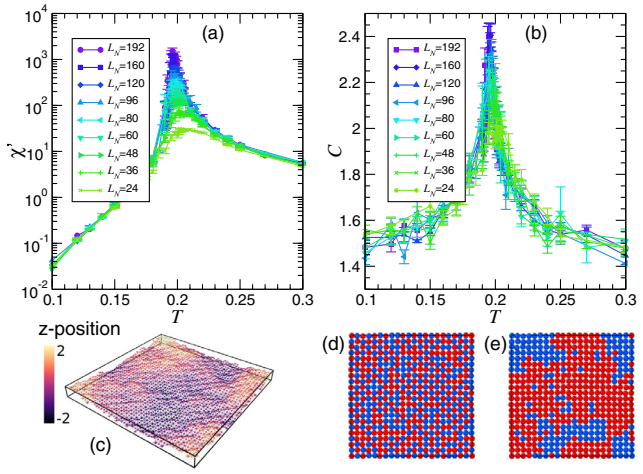

FIG. 3. (a) Staggered susceptibility χ' and (b) specific heat C as a function of temperature T for different system sizes for membranes with positive dilations. Plots for peaks as a function of system size and plots for membranes with negative dilations can be found in the Supplemental Material, Sec. VI [42]. (c) Snapshot of a fluctuating puckered surface close to T_c. (d) Top view of up(down) buckled sites [red(blue)] and (e) the corresponding staggered spin configuration for the surface pictured in (c).

by a constant factor above the transition and does not affect the susceptibility exponents [57,58]. See the Supplemental Material, Sec. VI [42] for details. We also calculate the specific heat per site as $C = (1/Nk_BT^2)(\langle E^2 \rangle - \langle E \rangle^2)$. This measurement uses the *total* potential energy, so N includes all sites.

The staggered susceptibility and specific heat of membranes with positive dilations as a function of T for a wide range of system sizes are shown in Fig. 3. We see that χ' and C reach maxima at $T \simeq 0.2$ and the peaks increase with system size, a signature of phase transitions in finite systems. Similar results for membranes with negative dilations appear in the Supplemental Material, Sec. VI [42]. In finite systems, the correlation length $\xi \sim |T - T_c|^{-\nu}$ cannot exceed the system size and thus the diverging quantities will reach a maximum when $\xi \simeq L$. Finite size scaling allows us to extract critical exponents [57–59].

Upon fitting the data with power law functions, we measure $\gamma/\nu = 1.741 \pm 0.062$, $\alpha/\nu = 0.068 \pm 0.018$ for $\Omega_0 > 0$ and $\gamma/\nu = 1.684 \pm 0.061$, $\alpha/\nu = 0.074 \pm 0.016$ for $\Omega_0 < 0$. The measurement of γ/ν is consistent with the rigid 2D Ising model value, 7/4. The value of α/ν, on the other hand, appears to be approximately four standard deviations away from 0, the 2D Ising expectation. Although our specific heat data cannot completely exclude a rigid Ising model logarithmic divergence in the specific heat, this observation suggests that the universality class is not 2D Ising. We can plausibly attribute this departure to the long-range interaction between staggered magnetization and Gaussian curvature that arises in the phenomenological model introduced in the following section. In the Supplemental Material, Sec. VI [42], we extract ν and present data for the exponents α, γ, and β.

Anomalous thermal expansion.—The order-disorder transition has a striking effect on the thermal expansion of the membrane as a function of temperature. We first examine the thermal contraction of a pristine membrane (no dilations) to establish a point of comparison. Thermalized membranes have been studied extensively using MD and Monte Carlo simulations [28–30,39,40,60,61], and their negative coefficient of thermal expansion α_T has been calculated analytically [62].

$$\alpha_T = \frac{1}{A_0}\frac{dA}{dT} \simeq -\frac{k_B}{4\pi\kappa}\left[\ln\left(\frac{l_{\rm th}}{a_0}\right) + \frac{1}{\eta} - \frac{1}{2}\right], \qquad (2)$$

where the thermal length $l_{\rm th} \equiv (\pi/q_{\rm th}) = \sqrt{(16\pi^3\kappa^2/3Yk_BT)}$ and η is a universal scaling exponent describing flexural phonons, $\eta \approx 0.8$ [62]. In our simulations, we vary T from 0.100 to 0.400, which varies $l_{\rm th}$ from $\sim 3.5a_0$ to $1.8a_0$. Figure 4(a) shows the average projected area divided by the area of a flat membrane as a function of T. Upon computing $\alpha_T = (1/A_0)(dA/dT)$, we find excellent agreement with Eq. (2) with no free parameters [red dashed line in Fig. 4(d)], using the zero-temperature values of the bending rigidity and Young's modulus. The pristine membrane model therefore reproduces the negative coefficient of thermal expansion of materials such as graphene [63]. In contrast, positive thermal expansion has been measured in

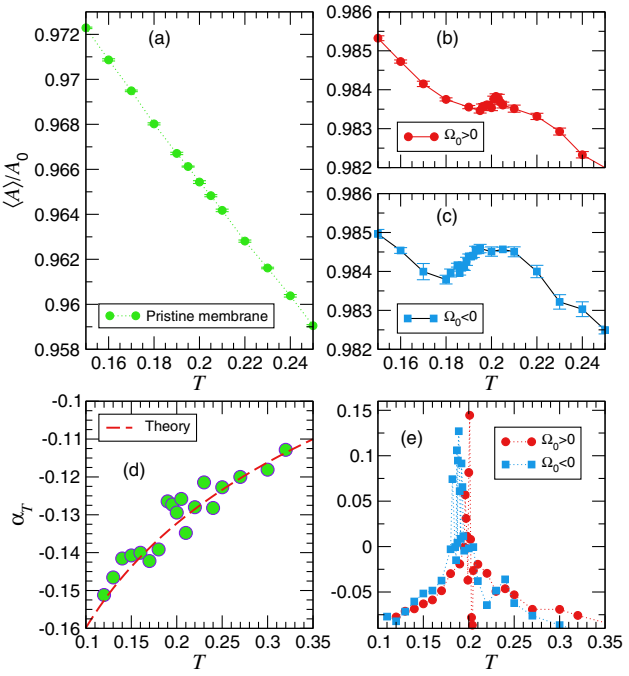

FIG. 4. Top row: Normalized area $\langle A\rangle/A_0$ as a function of T for (a) pristine membranes, (b) membranes with positive dilations, and (c) membranes with negative dilations for $L_N = 120$. $\langle A\rangle/A_0$ decreases with increasing T for pristine membranes whereas $\langle A\rangle/A_0$ for puckered membranes shows non-monotonic behavior. Bottom row: The coefficient of thermal expansion α_T as a function of T for (d) pristine membranes and (e) membranes with dilations. The theoretical prediction of α_T for pristine membranes with *no* adjustable fitting parameters matches very well with simulations (red dashed line). Far below T_c, α_T for membranes with dilations is negative, as for pristine membranes. Close to T_c, α_T increases rapidly and reaches a *positive* value, decreasing again to a negative value for T well above T_c.

relatively thick free-standing transition metal dichalcogenides, possibly due to a higher bending rigidity suppressing flexural phonons [41,64–66].

In contrast, $\langle A\rangle/A_0$ (and hence α_T) for puckered membranes shows nonmonotonic behavior. Here, the constant factor A_0 is the projected area of the lowest energy state at $T = 0$, a buckled checkerboard as described above. We observe that, while there is shrinkage for $T < T_c$ as for a pristine membrane, the value of α_T is less strongly negative. For $T \ll T_c$, $\alpha_T^{\text{puckered}}/\alpha_T^{\text{pristine}} \sim 0.5$, suggesting that membranes with ordered puckers stiffen. This observation is consistent with a theoretical argument based on Ref. [67], treating the buckled dilation texture as a frozen background metric (Supplemental Material [42], Sec. II). The calculation predicts the existence of an increased bending rigidity at $T = 0$, $\kappa_R \approx \kappa[1 + (3Yh_0^2/32\kappa)]$, where h_0 is the amplitude of the buckled membrane. Close to the transition, however, α_T increases rapidly and eventually reaches a *positive* value. Evidently, the swelling due to disordered up and down puckers on all length scales near T_c dominates the entropic shrinkage present in pristine sheets [62–64].

Phenomenological model.—To better understand the observed differences between the thermal expansion of pristine membranes and membranes with dilations, we introduce a "flexural Ising model," with an effective free energy that couples an Ising order parameter to a thin elastic sheet that is allowed to fluctuate both in and out of the plane. We assume coarse-graining such that the short wavelength, impurity-scale phonons are accounted for by a staggered pucker order parameter m_{st}, which interacts with a long wavelength nonlinear strain matrix, u_{ij}.

$$F = \int d^2x \left[\frac{\kappa}{2}(\nabla^2 f)^2 + \mu u_{ij}^2 + \frac{\lambda}{2}u_{kk}^2 + \frac{K}{2}(\nabla m_{\text{st}})^2 + \frac{r}{2}m_{\text{st}}^2 + u m_{\text{st}}^4 + g m_{\text{st}}^2 u_{kk}\right], \tag{3}$$

where u_{ij} is related to in-plane displacements u_j and out-of-plane displacements f by $u_{ij} = (1/2)[(\partial u_i/\partial x_j) + (\partial u_j/\partial x_i) + (\partial f/\partial x_i)(\partial f/\partial x_j)]$ [68]. The term proportional to g is the lowest order contribution allowed by symmetry coupling the phonon and order parameter fields. Similar free energies have been used to study flat compressible 2D Ising models in the limit $f = 0$ [69,70]. We also note similarities to free energies used to model electron-phonon interactions in graphene [71–74].

Upon tracing out the in-plane phonons according to standard methods [69,70,75], Eq. (3) becomes

$$\begin{aligned} F_{\text{eff}} = {} & \frac{g^2}{2A_0}\left(\frac{1}{2\mu+\lambda} - \frac{1}{\mu+\lambda}\right)\left(\int d^2x m_{\text{st}}^2\right)^2 \\ & + \int' d^2x \left[\frac{Y}{8}(P_{ij}^T \partial_i f \partial_j f)^2 + \frac{g\mu}{2\mu+\lambda}(m_{\text{st}}^2 P_{ij}^T \partial_i f \partial_j f)\right] \\ & + \int d^2x \left[\frac{\kappa}{2}(\nabla^2 f)^2 + \frac{K}{2}(\nabla m_{\text{st}})^2 + \frac{r}{2}m_{\text{st}}^2 \right. \\ & \left. + \left(u - \frac{g^2}{2(2\mu+\lambda)}\right)m_{\text{st}}^4\right], \end{aligned} \tag{4}$$

where P_{ij}^T is the transverse projection operator and the primed integral omits $\mathbf{q} = 0$ modes. Equation (4) has three terms that are not present for either pristine membranes or the Ising model. The first and final terms, proportional to g^2, also appear for flat compressible 2D Ising models [69,76]. The term proportional to g, however, is unique to the flexural Ising model. Since the Laplacian of $-\frac{1}{2}P_{ij}^T \partial_i f \partial_j f$ is the Gaussian curvature $S(\mathbf{x})$ in the Monge representation [77], this term represents a long-range interaction between the squared staggered magnetization and the Gaussian curvature of the form $(1/2\pi)\int d^2x \int d^2x' m_{\text{st}}{}^2(\mathbf{x})S(\mathbf{x}')\ln(|\mathbf{x}-\mathbf{x}'|)$. A power counting argument suggests that the coefficient

$w \equiv [g\mu/(2\mu+\lambda)]$ is a strongly relevant operator. We plan to examine the behavior of w in more detail in future work.

We can calculate the coefficient of thermal expansion α_T by adding an in-plane pressure, and compare to the simulation data in Fig. 4. As shown in Sec. I of the Supplemental Material, we find the average change in area

$$\langle \delta A \rangle = -\frac{gA_0\langle m_{\mathrm{st}}^2\rangle}{\mu+\lambda} - \frac{A_0}{2}\left\langle \left(\frac{\partial f}{\partial x_i}\right)^2 \right\rangle, \tag{5}$$

and coefficient of thermal expansion

$$\alpha_T = \frac{1}{A_0}\frac{dA}{dT} = -\frac{d}{dT}\left(\frac{g\langle m_{\mathrm{st}}^2\rangle}{\mu+\lambda}\right) - \frac{d}{dT}\left\langle \frac{1}{2}\left(\frac{\partial f}{\partial x_i}\right)^2 \right\rangle. \tag{6}$$

We expect that the microscopic couplings g and $\mu+\lambda$ depend only weakly on temperature over the temperature range of interest, provided we are far below the high temperature crumpling transition. Therefore, the contribution from the first term is sharply peaked around T_c, given the results in Fig. 2. We expect $g > 0$, as the antiferromagnetic state has a smaller projected area than the ferromagnetic state at $T = 0$, consistent with the positive peak in α_T at T_c observed in Fig. 4(e). The second term is the usual entropic thermal shrinkage, also present for a pristine membrane [62].

Conclusion.—We observe a phase transition in the staggered magnetization of a puckered membrane, which provides a mechanical analog of a highly compressible antiferromagnetic Ising model. Furthermore, we find that the order-disorder transition produces an anomalous thermal response for puckered membranes. These observations suggest a strong coupling between flexural phonons and the ordering of the spins (buckled sites). We introduce a phenomenological "flexural Ising model" that anticipates a competing effect between entropic shrinkage due to out-of-plane deformations and swelling due to pucker disorder at the phase transition.

Our findings suggest that bistable buckled structures change the thermal response of 2D materials, leading to a tunable coefficient of thermal expansion. The ability to tune thermal expansion is important for combining different materials, as mismatched thermal expansion can affect the longevity of integrated materials [78]. Materials with tunable thermal expansion are rare and often require precise engineering [34].

Since the phase transition temperature in our model depends on the elastic constants of the host lattice and the separation between dilations, one could imagine constructing a nanocantilever or nanoactuator out of a puckered membrane designed to be insensitive to thermal expansion or shrinkage at the temperature at which it must work ($\alpha_T = 0$ at two temperatures, one above and one below T_c). Additionally, the mechanism of an inefficient packing of buckled structures resulting in a global expansion can be applied to macroscale materials with multistable units [10,12,35]. Moreover, our work suggests the possibility of studying novel universality classes in 2D materials with a coupling between spin and both in-plane and out-of-plane displacements, generalizing past work on compressible Ising models to include flexural phonons.

P. Z. H., A. P., and D. R. N. acknowledge support through the NSF Grant No. DMR-1608501 and via the Harvard Materials Science Research and Engineering Center, through NSF Grant No. DMR-2011754. P. Z. H., A. P., and D. R. N. thank Suraj Shankar for helpful discussions. P. Z. H. also thanks Adam Iaizzi for helpful comments.

*paul.hanakata@gmail.com

[1] B. Florijn, C. Coulais, and M. van Hecke, Phys. Rev. Lett. **113**, 175503 (2014).
[2] M. A. Dias, M. P. McCarron, D. Rayneau-Kirkhope, P. Z. Hanakata, D. K. Campbell, H. S. Park, and D. P. Holmes, Soft Matter **13**, 9087 (2017).
[3] M. K. Blees, A. W. Barnard, P. A. Rose, S. P. Roberts, K. L. McGill, P. Y. Huang, A. R. Ruyack, J. W. Kevek, B. Kobrin, D. A. Muller, and P. L. McEuen, Nature (London) **524**, 204 (2015).
[4] P. Z. Hanakata, E. D. Cubuk, D. K. Campbell, and H. S. Park, Phys. Rev. Lett. **121**, 255304 (2018).
[5] P. Z. Hanakata, E. D. Cubuk, D. K. Campbell, and H. S. Park, Phys. Rev. Research **2**, 042006(R) (2020).
[6] S. Chen, J. Chen, X. Zhang, Z.-Y. Li, and J. Li, Light **9**, 1 (2020).
[7] B. Bircan, M. Z. Miskin, R. J. Lang, M. C. Cao, K. J. Dorsey, M. G. Salim, W. Wang, D. A. Muller, P. L. McEuen, and I. Cohen, Nano Lett. **20**, 4850 (2020).
[8] N. Oppenheimer and T. A. Witten, Phys. Rev. E **92**, 052401 (2015).
[9] C. Coulais, E. Teomy, K. De Reus, Y. Shokef, and M. Van Hecke, Nature (London) **535**, 529 (2016).
[10] J. A. Faber, J. P. Udani, K. S. Riley, A. R. Studart, and A. F. Arrieta, Adv. Sci. **7**, 2001955 (2020).
[11] A. Plummer and D. R. Nelson, Phys. Rev. E **102**, 033002 (2020).
[12] M. Liu, L. Domino, I. D. de Dinechin, M. Taffetani, and D. Vella, arXiv:2108.06499.
[13] J. L. Silverberg, J.-H. Na, A. A. Evans, B. Liu, T. C. Hull, C. D. Santangelo, R. J. Lang, R. C. Hayward, and I. Cohen, Nat. Mater. **14**, 389 (2015).
[14] S. Waitukaitis, R. Menaut, Bryan Gin-ge Chen, and M. van Hecke, Phys. Rev. Lett. **114**, 055503 (2015).
[15] J. T. Overvelde, T. A. De Jong, Y. Shevchenko, S. A. Becerra, G. M. Whitesides, J. C. Weaver, C. Hoberman, and K. Bertoldi, Nat. Commun. **7**, 10929 (2016).
[16] M. Stern, M. B. Pinson, and A. Murugan, Phys. Rev. X **7**, 041070 (2017).
[17] A. Molle, J. Goldberger, M. Houssa, Y. Xu, S.-C. Zhang, and D. Akinwande, Nat. Mater. **16**, 163 (2017).
[18] L. Seixas, A. S. Rodin, A. Carvalho, and A. H. Castro Neto, Phys. Rev. Lett. **116**, 206803 (2016).

[19] M. Singh, E. Della Gaspera, T. Ahmed, S. Walia, R. Ramanathan, J. van Embden, E. Mayes, and V. Bansal, 2D Mater. **4**, 025110 (2017).

[20] A. Pacheco-Sanjuan, T. B. Bishop, E. E. Farmer, P. Kumar, and S. Barraza-Lopez, Phys. Rev. B **99**, 104108 (2019).

[21] P. Z. Hanakata, A. S. Rodin, A. Carvalho, H. S. Park, D. K. Campbell, and A. H. Castro Neto, Phys. Rev. B **96**, 161401 (R) (2017).

[22] Q. Li, V. S. C. Kolluru, M. S. Rahn, E. Schwenker, S. Li, R. G. Hennig, P. Darancet, M. K. Chan, and M. C. Hersam, Science **371**, 1143 (2021).

[23] T. Daeneke, P. Atkin, R. Orrell-Trigg, A. Zavabeti, T. Ahmed, S. Walia, M. Liu, Y. Tachibana, M. Javaid, A. D. Greentree *et al.*, ACS Nano **11**, 10974 (2017).

[24] M. T. Lusk and L. D. Carr, Phys. Rev. Lett. **100**, 175503 (2008).

[25] T. Zhang, X. Li, and H. Gao, J. Mech. Phys. Solids **67**, 2 (2014).

[26] B. F. Grosso and E. J. Mele, Phys. Rev. Lett. **115**, 195501 (2015).

[27] C. Hofer, V. Skakalova, M. R. Monazam, C. Mangler, J. Kotakoski, T. Susi, and J. C. Meyer, Appl. Phys. Lett. **114**, 053102 (2019).

[28] W. Gao and R. Huang, J. Mech. Phys. Solids **66**, 42 (2014).

[29] P. Z. Hanakata, S. S. Bhabesh, M. J. Bowick, D. R. Nelson, and D. Yllanes, Extreme Mech. Lett. **44**, 101270 (2021).

[30] A. Morshedifard, M. Ruiz-García, M. J. Abdolhosseini Qomi, and A. Košmrlj, J. Mech. Phys. Solids **149**, 104296 (2021).

[31] K. N. Kudin, G. E. Scuseria, and B. I. Yakobson, Phys. Rev. B **64**, 235406 (2001).

[32] R. J. Nicholl, H. J. Conley, N. V. Lavrik, I. Vlassiouk, Y. S. Puzyrev, V. P. Sreenivas, S. T. Pantelides, and K. I. Bolotin, Nat. Commun. **6**, 8789 (2015).

[33] R. J. T. Nicholl, N. V. Lavrik, I. Vlassiouk, B. R. Srijanto, and K. I. Bolotin, Phys. Rev. Lett. **118**, 266101 (2017).

[34] N. C. Burtch, S. J. Baxter, J. Heinen, A. Bird, A. Schneemann, D. Dubbeldam, and A. P. Wilkinson, Adv. Funct. Mater. **29**, 1904669 (2019).

[35] E. Boatti, N. Vasios, and K. Bertoldi, Adv. Mater. **29**, 1700360 (2017).

[36] B. K. Greve, K. L. Martin, P. L. Lee, P. J. Chupas, K. W. Chapman, and A. P. Wilkinson, J. Am. Chem. Soc. **132**, 15496 (2010).

[37] M. Mehboudi, B. M. Fregoso, Y. Yang, W. Zhu, A. Van Der Zande, J. Ferrer, L. Bellaiche, P. Kumar, and S. Barraza-Lopez, Phys. Rev. Lett. **117**, 246802 (2016).

[38] H. S. Seung and D. R. Nelson, Phys. Rev. A **38**, 1005 (1988).

[39] M. J. Bowick, A. Košmrlj, D. R. Nelson, and R. Sknepnek, Phys. Rev. B **95**, 104109 (2017).

[40] R. Roldán, A. Fasolino, K. V. Zakharchenko, and M. I. Katsnelson, Phys. Rev. B **83**, 174104 (2011).

[41] J. W. Jiang, Nanotechnology **25**, 355402 (2014).

[42] See Supplemental Material at http://link.aps.org/supplemental/10.1103/PhysRevLett.128.075902 for details on theoretical derivations, extracting critical exponents, simulations, and a supplementary video, which includes Refs. [43–49].

[43] W. T. Koiter and A. Van Der Heijden, *WT Koiter's Elastic Stability of Solids and Structures* (Cambridge University Press, Cambridge, UK, New York, NY, USA, 2009).

[44] A. Košmrlj and D. R. Nelson, Phys. Rev. X **7**, 011002 (2017).

[45] J. Paulose, G. A. Vliegenthart, G. Gompper, and D. R. Nelson, Proc. Natl. Acad. Sci. U.S.A. **109**, 19551 (2012).

[46] E. Bitzek, P. Koskinen, F. Gähler, M. Moseler, and P. Gumbsch, Phys. Rev. Lett. **97**, 170201 (2006).

[47] M. I. Katsnelson, *Graphene: Carbon in Two Dimensions* (Cambridge University Press, Cambridge, England, 2012).

[48] S. J. Stuart, A. B. Tutein, and J. A. Harrison, J. Chem. Phys. **112**, 6472 (2000).

[49] Lammps, http://lammps.sandia.gov (2012).

[50] A. Stukowski, Model. Simul. Mater. Sci. Eng. **18**, 015012 (2010).

[51] D. R. Nelson, Phys. Rev. B **27**, 2902 (1983).

[52] L. Radzihovsky and D. R. Nelson, Phys. Rev. A **44**, 3525 (1991).

[53] D. R. Nelson and L. Radzihovsky, Europhys. Lett. **16**, 79 (1991).

[54] Y. Kantor, Europhys. Lett. **20**, 337 (1992).

[55] J. A. Anderson, J. Glaser, and S. C. Glotzer, Comput. Mater. Sci. **173**, 109363 (2020).

[56] A. P. Young, *Everything You Wanted to Know About Data Analysis and Fitting but Were Afraid to Ask* (Springer, Berlin, 2015).

[57] K. Binder, Rep. Prog. Phys. **60**, 487 (1997).

[58] A. M. Ferrenberg and D. P. Landau, Phys. Rev. B **44**, 5081 (1991).

[59] A. W. Sandvik, in *AIP Conference Proceedings* (American Institute of Physics, 2010), Vol. 1297, pp. 135–338.

[60] D. Yllanes, S. S. Bhabesh, D. R. Nelson, and M. J. Bowick, Nat. Commun. **8**, 1381 (2017).

[61] D. Wan, D. R. Nelson, and M. J. Bowick, Phys. Rev. B **96**, 014106 (2017).

[62] A. Košmrlj and D. R. Nelson, Phys. Rev. B **93**, 125431 (2016).

[63] D. Yoon, Y.-W. Son, and H. Cheong, Nano Lett. **11**, 3227 (2011).

[64] X. Hu, P. Yasaei, J. Jokisaari, S. Öğüt, A. Salehi-Khojin, and R. F. Klie, Phys. Rev. Lett. **120**, 055902 (2018).

[65] S. Bertolazzi, J. Brivio, and A. Kis, ACS Nano **5**, 9703 (2011).

[66] G. Wang, Z. Dai, J. Xiao, S. Z. Feng, C. Weng, L. Liu, Z. Xu, R. Huang, and Z. Zhang, Phys. Rev. Lett. **123**, 116101 (2019).

[67] A. Košmrlj and D. R. Nelson, Phys. Rev. E **88**, 012136 (2013).

[68] L. D. Landau, A. Kosevich, L. P. Pitaevskii, and E. M. Lifshitz, *Theory of Elasticity* (Butterworth-Heinemann, Oxford, 1986).

[69] J. Sak, Phys. Rev. B **10**, 3957 (1974).

[70] A. Larkin and S. Pikin, Sov. Phys. JETP **29**, 891 (1969).

[71] D. Gazit, Phys. Rev. B **80**, 161406(R) (2009).

[72] F. Guinea, P. Le Doussal, and K. J. Wiese, Phys. Rev. B **89**, 125428 (2014).

[73] L. L. Bonilla and M. Ruiz-Garcia, Phys. Rev. B **93**, 115407 (2016).
[74] T. Cea, M. Ruiz-Garcia, L. L. Bonilla, and F. Guinea, Phys. Rev. B **101**, 235428 (2020).
[75] D. Nelson and L. Peliti, J. Phys. **48**, 1085 (1987).
[76] J. Bruno and J. Sak, Phys. Rev. B **22**, 3302 (1980).
[77] D. R. Nelson, T. Piran, and S. Weinberg, *Statistical Mechanics of Membranes and Surfaces* (World Scientific, Singapore, 2004).
[78] M. R. Werner and W. R. Fahrner, IEEE Transactions on Industrial Electronics **48**, 249 (2001).